



MEAN VELOCITY AND PRESSURE AND VELOCITY SPECTRAL  
MEASUREMENTS WITHIN A SEPARATED FLOW AROUND A  
PROLATE SPHEROID AT INCIDENCE

**AIAA-98-0630**

**Mean Velocity and Pressure and Velocity  
Spectral Measurements within a Separated  
Flow Around a Prolate Spheroid at Incidence**

M. Goody, R. L. Simpson, and M. Engel,  
C. Chesnakas, and W. Devenport  
Department of Aerospace and Ocean Engineering  
Virginia Polytechnic Institute and State University  
Blacksburg, VA

**36th Aerospace Sciences  
Meeting & Exhibit**  
January 12-15, 1998 / Reno, NV

For permission to copy or republish, contact the American Institute of Aeronautics and Astronautics  
1801 Alexander Bell Drive, Suite 500, Reston, Virginia 20191-4344

# MEAN VELOCITY AND PRESSURE AND VELOCITY SPECTRAL MEASUREMENTS WITHIN A SEPARATED FLOW AROUND A PROLATE SPHEROID AT INCIDENCE

Michael C. Goody\*  
 Roger L. Simpson†  
 Mark Engel‡  
 Christopher J. Chesnakas§  
 William J. Devenport ¶

Department of Aerospace and Ocean Engineering  
 Virginia Polytechnic Institute and State University  
 Blacksburg, Virginia 24061

## Abstract

Hot-wire velocity measurements were made on the lee-side of a 6:1 prolate spheroid,  $Re_L = 4.2 \times 10^6$ , at  $10^\circ$  and  $20^\circ$  angles of attack, and at  $x/L = 0.600$  and  $0.772$ . The dominant feature of each of these flowfields is the presence of a shed vortex due to cross-flow separation. This is a source of considerable noise and vibration. At  $\alpha = 10^\circ$  the most turbulent fluid is confined to the near wall region. At  $\alpha = 20^\circ$  the most turbulent fluid appears away from the wall at locations where the flow is separating. Velocity spectra for regions with weaker 3-D effects exhibit features that are observed for equilibrium flows. Spectra in strong vortical flow regions show unusual and apparently non-equilibrium behavior. This behavior has some qualitative similarities with surface pressure fluctuation spectra.

## Nomenclature

L Model length, 1.37 m.  
 p Pressure fluctuation at the model surface  
 $q_e$  Dynamic pressure at boundary layer edge

r Distance from model surface along a line perpendicular to the model axis  
 $Re_L$  Reynolds number,  $U_\infty L / \nu$   
 TKE Turbulent kinetic energy, defined as,  
 $TKE = \frac{1}{2} \rho (\overline{u^2} + \overline{v^2} + \overline{w^2})$   
 $u_\tau$  Friction velocity,  $(\tau_w / \rho)^{1/2}$   
 $u, v, w$  Fluctuating velocity components in the directions of U, V, and W, respectively  
 U Velocity component in a plane parallel to the surface, in the axial direction  
 $U_e$  Total velocity at edge of shear layer  
 $U_\infty$  Wind tunnel free-stream velocity  
 V Mean velocity component normal to the local model surface  
 W Mean velocity component in a plane parallel to the local model surface and perpendicular to the axial direction (positive in  $-\phi$  direction)  
 x Axial distance from the nose of the model  
 $y^+$   $ru/\nu$   
 $\alpha$  Angle of attack of model relative to incoming flow  
 $\delta$  Boundary layer thickness  
 $\delta^*$  Boundary layer streamwise displacement thickness, defined as

$$\delta^* = \int_0^\delta \left[ 1 - \frac{(U^2 + W^2)^{1/2}}{(U^2 + W^2)_e^{1/2}} \right] dr$$

$\nu$  Kinematic viscosity of flow  
 $\rho$  Mass density of flow  
 $\tau_w$  Shear stress magnitude at the surface of the model  
 $\phi$  Circumferential coordinate, from windward side

\* Graduate Assistant, Student Member AIAA  
 † Jack E. Cowling Professor, Fellow AIAA  
 ‡ Former Graduate Assistant  
 § Member AIAA, now at  
 David Taylor Model Basin CD/NSWC,  
 Bethesda, MD  
 ¶ Associate Professor, Senior Member AIAA

Copyright © 1998 By M. Goody, R. Simpson, M. Engel, C. Chesnakas, and W. Devenport. Published by the American Institute of Aeronautics and Astronautics with permission.

- $\Phi$  Power spectrum of surface pressure fluctuations such that

$$\overline{p'^2} = \int_0^\infty \Phi(\omega) d\omega$$

- $\Phi_{ij}$  Power spectrum of velocity fluctuations such that

$$\overline{u_i u_j} = \int_0^\infty \Phi_{ij}(\omega) d\omega$$

- $\omega$  Circular frequency, radians

Primes denote the root mean square value of fluctuating quantities

## Introduction

The flow about a 6:1 prolate spheroid exhibits fundamental open separation phenomena of three-dimensional flow (Figure 1). It is reflected by the convergence of skin friction lines. The flow separating from the lee-side rolls up into a strong vortex on each side of the body. This primary vortex may be accompanied by one or more smaller vortices, each of which is associated with a separation and reattachment line. The complex interactions between vortices result in a highly skewed three-dimensional shear layer. Simpson<sup>19,20</sup> treats three dimensional turbulent separation in detail.

The current study is part of an ongoing effort to extensively measure this flowfield in order to increase the understanding of the flow physics and to provide an experimental data base for comparison with computations. The effects of Reynolds number and angle of attack on boundary layer transition and separation were studied by Ahn and Simpson<sup>2</sup>. Barber and Simpson<sup>3</sup> documented the mean and fluctuating velocities in the cross-flow separation region, but the use of five-hole pressure probes and crossed hot wires precluded them from obtaining data within the inner boundary layer.

Previous studies of a tripped flow for angles of attack of 10° and 20° at a length Reynolds number  $Re_L = 4.2 \times 10^5$  by Chesnakas and Simpson<sup>4,8</sup> did not suffer this limitation. They thoroughly documented the turbulence structure, including all Reynolds stresses and velocity triple products, to  $y^+$  closer than 7. This was possible through the use of the specially designed, miniature fiber-optic LDV probe described in Chesnakas and Simpson<sup>5</sup>. Their experimental data have shown that this flowfield contains large regions in which the flow-

gradient angle and turbulent-shear-stress angle differ considerably. This anisotropic condition implies that popular turbulence models using the isotropic eddy viscosity formulation cannot be adapted to this flowfield while retaining important physical information. This has been confirmed in work reported by AGARD<sup>1</sup>, Gee et al.<sup>10</sup>, Sung et al.<sup>21</sup> and Ramamurti et al.<sup>17</sup>.

Chesnakas and Simpson<sup>7</sup> investigated the effects of three dimensionality on the turbulence structure of the 6:1 prolate spheroid. They focused one location ( $x/L = 0.762$ ,  $\phi = 123^\circ$ ) near separation<sup>22</sup> at one angle of attack ( $\alpha = 10^\circ$ ). Data were used to calculate important terms in the turbulent kinetic energy transport equation from the viscous sublayer to the boundary layer edge. They showed that the assumptions of several turbulence models were not supported by the measured flow conditions.

Goody et al.<sup>11</sup> measured surface pressure fluctuations and pressure-velocity fluctuations at 10° and 20° angle of attack and  $x/L = 0.600$  and  $x/L = 0.772$ . They also observed significant correlation between surface pressure and wall-normal velocity fluctuations for all locations except those between separation and the shed vortex that are near the wall. The  $p'$  is a local minimum where the flow separates and a local maximum where the flow reattaches<sup>23</sup>.

Elsewhere Meier et al.<sup>15,16</sup>, Kreplin et al.<sup>13,14</sup> and Vollmers et al.<sup>24</sup> at the DFVLR (now DLR) have documented the surface flow, mean surface pressure, skin friction, and mean velocity at several Reynolds numbers and angles of attack.

Four sensor hot-wire anemometer measurements of the outer layer flow are presented here to complement the near-wall, LDV measurements of Chesnakas et al.<sup>4,8</sup> They serve to document the outer layer features such as the vortices shed by cross flow separation. Additionally, measurements of velocity spectra are used to examine the turbulence structure of this flow and can be used for future comparison with large eddy simulations.

## Apparatus and Techniques

The measurements were made in the Virginia Polytechnic Institute and State University Stability Wind Tunnel. This tunnel is a continuous, closed return, subsonic wind tunnel with a 7 m long 1.8 m square test section. The precisely regulated d.c. power source, a 9:1 area contraction, and seven anti-turbulence screens provide low free-stream turbulence levels - on the

order of 0.03%. All measurements were conducted at  $Re_x = 4.20 \times 10^5$  and ambient temperature.

The 6:1 prolate spheroid used for these measurements is 1.37 m long and is constructed of a fiberglass skin bonded to an aluminum frame. A circumferential trip, consisting of posts 1.2 mm in diameter, 0.7 mm high and spaced 2.5 mm apart, was placed around the model at  $x/L = 0.2$ . This stabilized the location of transition. Windows  $30 \times 150 \times 0.75$  mm were placed in the skin for optical (LDV) access to the flow. The windows were molded to the curvature of the model and mounted flush with the model surface in order to minimize flow disturbances. Wax was used to fill any small gaps in the model surface. The model was supported with a rear-mounted, 0.75 m long sting connecting to a vertical post extended through the wind tunnel floor.

Even though no new LDV measurements are reported here, a brief description of the previous LDV setup is given since those data are compared with the hot-wire measurements. Near-wall velocity measurements were made using a three-component, fiber-optic LDV probe designed specifically for those experiments<sup>5</sup>. This probe is able to measure the complete velocity vector and full Reynolds stress tensor. Incident beams come from the blue and green lines of an argon-ion laser with scattered light collected in off-axis backscatter. Three orthogonal velocity components are measured coincidentally in space and time in a probe volume that is nearly spherical with a diameter of approximately 55  $\mu\text{m}$ . The probe was mounted inside the model with all beams passing through the window. It could be remotely traversed  $\pm 2.5$  cm in both the axial direction and normal to the major axis. Positioning in the circumferential direction ( $\phi$ ) was achieved by rotating the model about its major axis.

The Doppler frequency of each of the LDV signals was analyzed using 3 Macrodyne model FDP3100 frequency domain signal processors operating in coincidence mode. The flow was seeded using polystyrene latex spheres 0.7  $\mu\text{m}$  in diameter. The particle velocity and the pressure at the window pressure tap were sampled simultaneously and stored with 16-bit precision. The sample rate varied from 40 samples/sec near the surface to 250 samples/sec in the outer part of the measurement region.

Boundary layer velocity profiles were measured with the LDV at 10-14 circumferential locations from  $\phi = 90^\circ$  to  $\phi = 180^\circ$ . Each profile consisted of 17-19 radial locations from 0.007 cm above the model surface out to 2.5-3.0 cm. At each

of these locations 16,384 coincident 3-D velocity-pressure realizations were acquired.

In the new measurements reported here, a miniature 4-sensor hot-wire probe consisting of two orthogonal X-wire arrays (Auspex Corp. AVOP-4-100) was used. It has 5  $\mu\text{m}$  tungsten sensors 0.8 mm in length and a measurement volume of 0.5  $\text{mm}^3$ .

The hot-wire sensors were operated separately, each using a Dantec 56C17/56C01 anemometer unit. Anemometer outputs were read by an IBM AT compatible computer through an Analogic 12 bit HSDAS-12 A/D converter buffered by four  $\times 10$  buck-and-gain amplifiers. A traversing gear mounted in the wind tunnel allowed the horizontal and vertical position of the probe to be controlled from the computer. A probe holder positioned the tip of the probe well upstream of the traverse gear. The probe was held parallel to the free-stream direction for all velocity measurements. A detailed description of the hot-wire measurement system in addition to related calibration and reduction procedures is given by Devenport et al.<sup>9</sup> and Wittmer et al.<sup>24</sup>

Two sets of hot-wire measurements were made. The first set targeted the mean flow, Reynolds stresses and triple products. Velocity profiles were made at  $5^\circ$   $\phi$  increments (circumferential) from  $\phi = 130^\circ$ ,  $140^\circ$  to  $\phi = 180^\circ$ . Each profile consisted of 11-13 radial locations from 0.60-0.75 cm above the model surface to 8-12 cm.

The second set was used to obtain velocity spectra. Fifty records of 6144 samples were acquired at 50 kHz at selected locations (see Table 1). The period for each continuous record was at least 1 second in order to capture low frequency fluctuations.

Measurements were made at two axial locations,  $x/L = 0.600$  and  $x/L = 0.772$ , at each of two angles of attack,  $\alpha = 10^\circ$  and  $\alpha = 20^\circ$ . This gives a total of four measurement stations.

## Uncertainty Estimates

The uncertainty in mean velocity measurements is within 0.015- $U_c$ . The circumferential position was measured with a sting-mounted vernier-type scale and is certain to within 0.1°. A detailed discussion of the uncertainty of the LDV measurements is given by Chesnakas<sup>7</sup>. Uncertainties associated with the four sensor hot-wire measurement system is given by Devenport et al.<sup>9</sup> and Wittmer et al.<sup>24</sup> Small alignment corrections were applied to the hot-wire

anemometer data. Secondary flow streamlines in show good agreement between the hot-wire anemometer data and earlier reported LDV data taken near the model surface.

## Results

The velocity components are presented here as  $U, V, W$  in the Body Surface coordinate system. This is different than the Body Axis coordinate system which uses  $x, r, \phi$  to define position. The difference is shown in Figure 2. In the Body Axis coordinate system  $x$  is the distance from the nose of the model measured along the model axis. The radial distance,  $r$ , from the surface of the model is measured perpendicular to the model axis. The azimuthal position,  $\phi$ , is measured from the windward side of the model. In the Body Surface coordinate system  $U$  is tangent to the model surface and points toward the tail of the model;  $V$  is normal to the model surface, positive outward; and  $W$  is tangent to the model surface, positive windward, to form a right-handed coordinate system. The transformation from the Body Axis coordinate system to the Body Surface coordinate system is a rotation about the  $\phi$  axis. The rotations required are  $1.948^\circ$  and  $6.167^\circ$  at  $x/L = 0.600$  and  $x/L = 0.772$ , respectively.

This investigation serves to document outer layer features such as vortices shed by cross-flow separation. Even though measurements at  $\alpha = 10^\circ, x/L = 0.772$  and  $\alpha = 20^\circ, x/L = 0.600$  were also obtained, only those at  $\alpha = 10^\circ, x/L = 0.600$  and  $\alpha = 20^\circ, x/L = 0.772$  are presented here. The flowfield at  $\alpha = 10^\circ, x/L = 0.600$  is only starting to separate and the turbulence structure is closest to that of an equilibrium turbulent flow. The flowfield at  $\alpha = 20^\circ, x/L = 0.772$  contains strong separations and has a high degree of three-dimensionality both in the mean flow and turbulence structure. Near-wall LDV measurements for all 4 stations can be found elsewhere<sup>8</sup>. Secondary flow streamlines interpolated from  $V, W$  data at the latter measurement stations are shown in Figure 3, 8, and 9. The mean flow field at all measurement stations shows cross flow separation and a shed vortex. Between the separation and shed vortex is a trough of low velocity fluid<sup>8</sup>.

The secondary flowfield with contours of TKE at  $\alpha = 10^\circ, x/L = 0.600$  is shown in Figure 3. The mean flow separates at  $\phi = 145^\circ$  and a weak vortex forms at  $\phi = 162^\circ$  approximately 0.375 cm above the wall. This separation is not strong. Previously measured surface pressure spectra<sup>11</sup>

collapse at low frequencies when scaled on  $\delta^*, U_{\infty}$ , and  $q_w$  (Figure 4). This collapse is also observed in  $\Phi_{11}(\omega)/U_{\infty}\delta^*$  for  $150^\circ < \phi < 170^\circ$  (Figure 5). This is to be expected since the weak separation was found to have little effect on  $U$  and  $u'$  at the locations where spectra were obtained. Figures 6 and 7 show a slight decrease in  $\Phi_{22}(\omega)/U_{\infty}\delta^*$  and  $\Phi_{33}(\omega)/U_{\infty}\delta^*$  at low frequencies from  $\phi = 150^\circ$  to  $\phi = 170^\circ$ . Features of these spectra are observed in equilibrium turbulent flows.

The secondary flowfield at  $\alpha = 20^\circ, x/L = 0.772$  is shown in Figures 8 and 9. There is a primary separation at  $\phi = 115^\circ$  and an associated primary vortex at  $r = 3$  cm,  $\phi = 155^\circ$ . There is also a secondary separation at  $\phi = 145^\circ$  and downflow at  $\phi = 135^\circ$  which is associated with a secondary vortex at approximately  $r = 0.6$  cm,  $\phi = 140^\circ$ . Contours of the local mean velocity magnitude are shown in Figure 8. They show the low velocity trough (first reported by Chesnakas et al.<sup>8</sup>) between the separation location and associated vortex. This trough extends out a significant distance from the wall. Diminished mean flow gradients and Reynolds shear stresses within this trough cause TKE to be low there, due to diminished TKE production. However, at the edges of the trough mean velocity gradients are high. This combined with elevated Reynolds stresses increase TKE production. This is most evident at the top of the low velocity trough ( $\phi = 140^\circ, r = 2.75$  cm,  $y^+ = 3993$ ) where the highest TKE ( $= 0.022\rho U_{\infty}^2$ ) was measured. The main contribution to this high TKE is  $\overline{w'^2}$  ( $= 0.022U_{\infty}^2$ ) as compared to  $\overline{u'^2}$  ( $= 0.012U_{\infty}^2$ ) and  $\overline{v'^2}$  ( $= 0.009U_{\infty}^2$ ). Also notable is that the Reynolds shear stresses are maximum at this location.

Previously measured surface pressure fluctuation spectra<sup>11</sup> do not collapse at this measurement station when scaled on  $\delta^*, U_{\infty}$ , and  $q_w$  (Figure 10). This is also true for the velocity spectra scaled on  $\delta^*$  and  $U_{\infty}$  (Figures 11 - 13). However, the velocity spectra show unusual features that seem to follow the surface pressure fluctuations. Since the velocity spectra at  $\alpha = 10^\circ, x/L = 0.600$  appear to demonstrate the validity of the experimental methods, we have confidence in the validity of these latter data.

The locations  $r = 0.6$  cm,  $\phi = 135^\circ, 140^\circ$ , and  $145^\circ$  traverse the secondary vortex. A hump is observed in  $\Phi_{33}(\omega)/U_{\infty}\delta^*$  at low and middle frequencies. Although the frequency about which this hump is centered does not scale on  $\delta^*$  and  $U_{\infty}$ , it is confined to the range  $0.2 < \omega\delta^*/U_{\infty} < 0.6$ . The most dominant variation in  $\Phi_{11}(\omega)/U_{\infty}\delta^*$  appears to correlate with the secondary separation (at  $\phi = 145^\circ$ ) and downflow (at  $\phi = 135^\circ$ ). The

value of  $\Phi_{11}(\omega)/U_c \delta^*$  decreases in the middle frequency range as  $\phi$  goes from the downflow location to the separation location. A substantial decrease is observed in  $\Phi_{22}(\omega)/U_c \delta^*$  at the secondary separation location for all but the highest frequencies. It is noted that Wetzel<sup>23</sup> found  $p'$  to be a local minimum at separation. The locations  $r = 3.0$  cm,  $\phi = 135^\circ, 140^\circ, 150^\circ$  traverse the region of highest TKE. The spectral values of all three velocity components increase (with the TKE) over the entire frequency range.

The spectra of all three velocity components contain some range that decays as  $\omega^{-5/3}$  for all of the measurement stations. This is most evident at the  $\alpha = 20^\circ$  stations. This relationship was approached tangentially at  $\alpha = 10^\circ$ . This power law relationship is indicative of the inertial subrange which follows from Kolmogorov's second hypothesis<sup>12</sup> of universal statistical equilibrium for sufficiently high Reynolds number. This, however, was not found to be the case here. Other relationships resulting from universal statistical equilibrium, such as  $E_{22}(k_1) = E_{33}(k_1) = 4/3 E_{11}(k_1)$ , are not satisfied by this data.

The velocity spectra are presented here non-dimensionalized using  $\delta^*$  and  $U_c$ . It is evident from Figures 5 - 7 and 11 - 13 that this does not collapse the spectra. Unsuccessful attempts were made to collapse the spectra. These included using the following length scale and velocity scale combinations:  $r, U_c; \delta^*,$  local mean velocity;  $r,$  and local mean velocity. It was found that  $\Phi_{11}(\omega), \Phi_{22}(\omega),$  and  $\Phi_{33}(\omega)$  each need a different scaling in order to collapse. This means that flow parameters such as  $r, \delta^*, U_c,$  and  $\psi$  which are independent of velocity component will not work for all of the spectra. Additionally, the spectra were analyzed expressed in a Local Streamline coordinate system. This attempt to collapse the spectra was also unsuccessful.

## Conclusions

Mean velocity and Reynolds stresses were measured and velocity spectra were obtained using a four sensor hot-wire anemometer. In regions of overlap with the previously measured LDV data the secondary flow patterns show good agreement. Velocity spectra for regions with weaker 3-D effects exhibit features that are observed for equilibrium flows. Spectra in strong vortical flow regions show unusual and apparently non-equilibrium behavior. This behavior has some qualitative similarities with surface pressure fluctuation spectra.

## Acknowledgements

The authors appreciate the support of the Office of Naval Research under Grant N00014-94-1-0092 and AASERT Grant N00014-94-1-0802, Dr. L. P. Purtell, Program Manager.

## References

- AGARD, AGARD-AR-255, Neuilly sur Seine, FR (1991).
- Ahn, S. and Simpson, R. L., AIAA-91-0428, 30th Aero Sci Meeting, Reno, NV (6-9 Jan 1992).
- Barber, K. M. and Simpson, R. L., AIAA-91-0255, 29th Aero Sci Meeting, Reno, NV (7-10 Jan 1991).
- Chesnakas, C. J., Simpson, R. L., Madden, M. M., Data Report VPI-AOE-202REV, Dept. Of Aero & Ocean Engr, VPI&SU, DTIC:AOA2764850XSP, Blacksburg, VA (Jan 1994).
- Chesnakas, C. J. and Simpson, R. L., *Exp Fluids*, 17, pp. 68-74, 1994.
- Chesnakas, C. J. and Simpson, R. L., AIAA-96-0320, 34th Aero Sci Meeting, Reno, NV (15-18 Jan 1996).
- Chesnakas, C. J. and Simpson, R. L., *J Fluid Engr*, 118, pp. 268-275, 1996.
- Chesnakas, C. J. and Simpson, R.L., *AIAA J*, 35, pp. 990-999, 1997.
- Devenport, W. J., Rife, M. C., Liapis, S. I., Follin, G. J., *J. Fluid Mech.*, 332, pp. 71-104, 1997.
- Gee, K., Cummings, R. M., Schiff, L. B., *AIAA J*, 30, pp. 655-664, 1992.
- Goody, M. C., Simpson, R. L., Chesnakas, C. J., AIAA-97-0485, 35th Aero. Sci. Meeting, Reno, NV (6-10 Jan 1997).
- Kolmogorov, A. N., *C. R. Acad. Sci. URSS*, 30, p. 301, 1941.
- Kreplin, H. P., Vollmers, H., Meier, H. U., Data Report DFVLR 1B 222-84/A 33, Göttingen (1985).
- Kreplin, H. P. and Stäger, R., Paper 2-4, 9th Symp Turb Shear Flow, Kyoto, Japan (16-18 Aug 1993).
- Meier, H., Kreplin, H., Landauffer, A., Baumgarten, D., Data Report DFVLR 1B 222-4/A10, Göttingen (1994).
- Meier, H. U., Kreplin, H. P., Landauffer, A., Data Report DFVLR 1B 222-86/A 04, Göttingen (1985).
- Ramamurti, R., Sandberg, W., Löhner, R., AIAA-94-0756, 32nd Aero Sci Meeting, Reno, NV (10-13 Jan 1994).
- Simpson, R. L., *Ann Rev of Fluid Mech*, 21, pp. 205-234, 1989.
- Simpson, R. L., AIAA-95-0226, 33rd Aero Sci Meeting, Reno, NV (9-12 Jan 1995).
- Simpson, R. L., *Progress in Aerospace Sciences*, 32, pp. 457-521, 1996.
- Sung, C. H., Griffin, M. J., Tsai, J. F., Huang, T. T., AIAA-93-0787, 31st Aero Sci Meeting, Reno, NV (11-14 Jan 1993).
- Vollmers, H., Kreplin, H. P., Meier, H. U., Paper 14, AGARD-CP-342, *Aerodynamics of Vortical-Type Flows in Three Dimensions* (1983).
- Wetzel, T. G., Simpson, R. L., Chesnakas, C. J., accepted *AIAA J*, 1998.
- Wittmer, K. S., Devenport, W. J., Zsoldos J. S., *Exp. In Fluids*, 24, pp. 769-786, 1998.

$\alpha$	$x/L$	$r$ (cm)	$\phi$	$\delta'$ (cm)	$v$ (m/s)	$u$ (m/s)	$U$ (m/s)
10°	0.600	0.75	150°	0.376	$1.857 \times 10^3$	1.93	57.02
			155°	0.365	$1.859 \times 10^3$	1.95	56.88
			160°	0.355	$1.861 \times 10^3$	1.98	56.92
			165°	0.330	$1.862 \times 10^3$	2.03	57.11
			170°	0.305	$1.863 \times 10^3$	2.08	57.58
10°	0.772	1.00	120°	0.331	$1.804 \times 10^3$	1.75	56.27
			130°	0.562	$1.809 \times 10^3$	1.55	58.10
			135°	0.639	$1.812 \times 10^3$	1.52	57.64
			140°	0.733	$1.814 \times 10^3$	1.55	57.02
			150°	0.716	$1.814 \times 10^3$	1.78	55.71
			160°	0.447	$1.818 \times 10^3$	2.04	53.77
			165°	0.337	$1.821 \times 10^3$	2.14	54.34
			170°	0.267	$1.822 \times 10^3$	2.24	55.07
20°	0.600	0.60	125°	0.330	$1.795 \times 10^3$	1.52	54.43
			130°	0.498	$1.799 \times 10^3$	1.39	54.13
			135°	0.594	$1.800 \times 10^3$	1.83	53.91
			140°	0.624	$1.802 \times 10^3$	2.05	53.69
		2.00	145°	0.547	$1.805 \times 10^3$	2.03	60.56
			140°	0.624	$1.788 \times 10^3$	2.05	53.49
			150°	0.437	$1.786 \times 10^3$	2.62	58.75
			155°	0.434	$1.782 \times 10^3$	3.11	55.98
20°	0.772	0.60	160°	0.400	$1.753 \times 10^3$	3.20	51.90
			135°	0.608	$1.810 \times 10^3$	2.45	51.71
			140°	0.488	$1.817 \times 10^3$	2.63	50.26
		1.00	145°	0.640	$1.819 \times 10^3$	1.83	56.42
			130°	0.728	$1.809 \times 10^3$	2.29	57.63
		3.00	135°	0.608	$1.812 \times 10^3$	2.45	57.02
			135°	0.608	$1.814 \times 10^3$	2.45	57.02
			140°	0.488	$1.816 \times 10^3$	2.63	50.08
			150°	0.529	$1.823 \times 10^3$	2.23	57.88
155°	0.352	$1.825 \times 10^3$	3.10	56.52			
160°	0.260	$1.825 \times 10^3$	3.32	56.11			

Table 1- Velocity spectra measurement locations with some mean flow properties

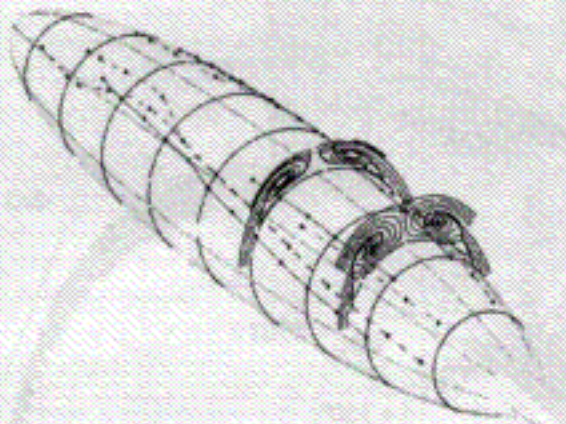


**Figure 1 -** Flowfield about a 6:1 prolate spheroid at  $\alpha = 20^\circ$ ,  $x/L = 0.600$  and  $0.772$ . Solid lines on model surface show separation lines from oil-flow visualization. Dashed lines show minima in skin friction. (From Wetzel et al.<sup>20</sup>)

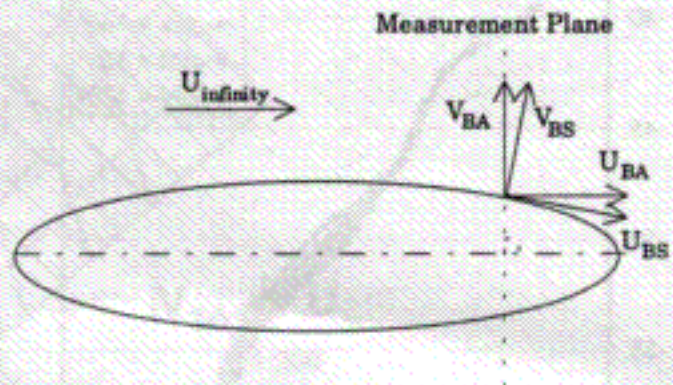


**Figure 2 -** Relationship between Body Axis coordinate system and Body Surface coordinate system

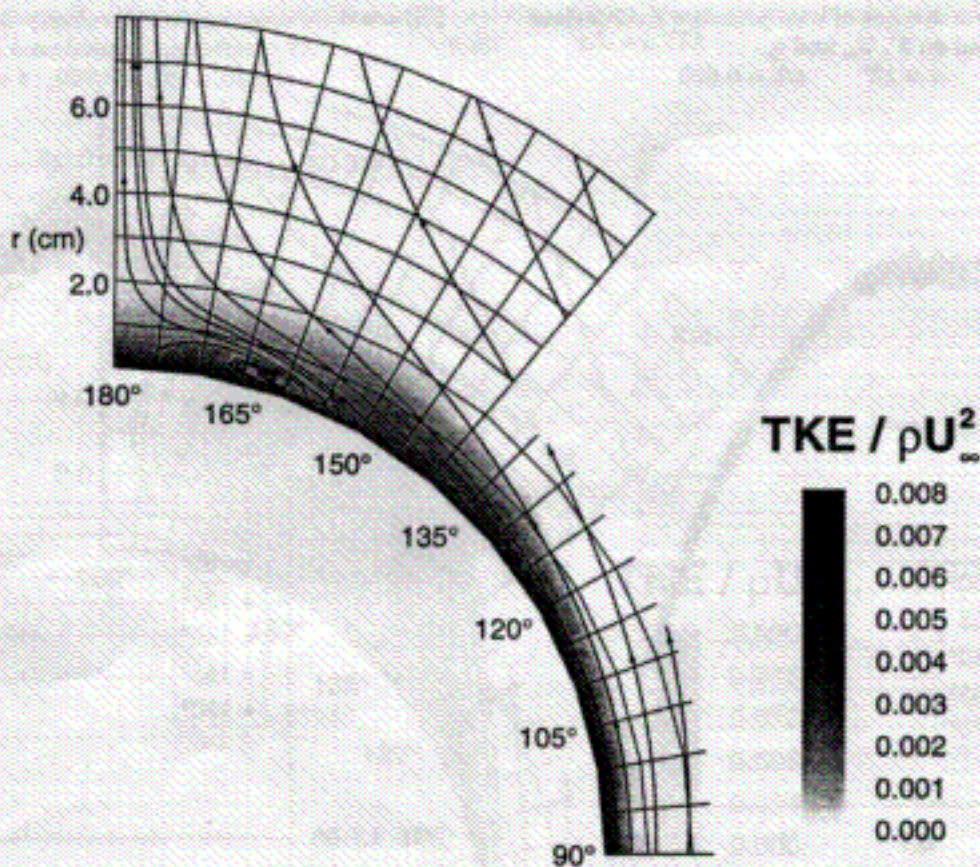


**Figure 3 -** Secondary streamlines with contours of  $TKE / \rho U_\infty^2$   
 $\alpha = 10^\circ$   $x/L = 0.600$

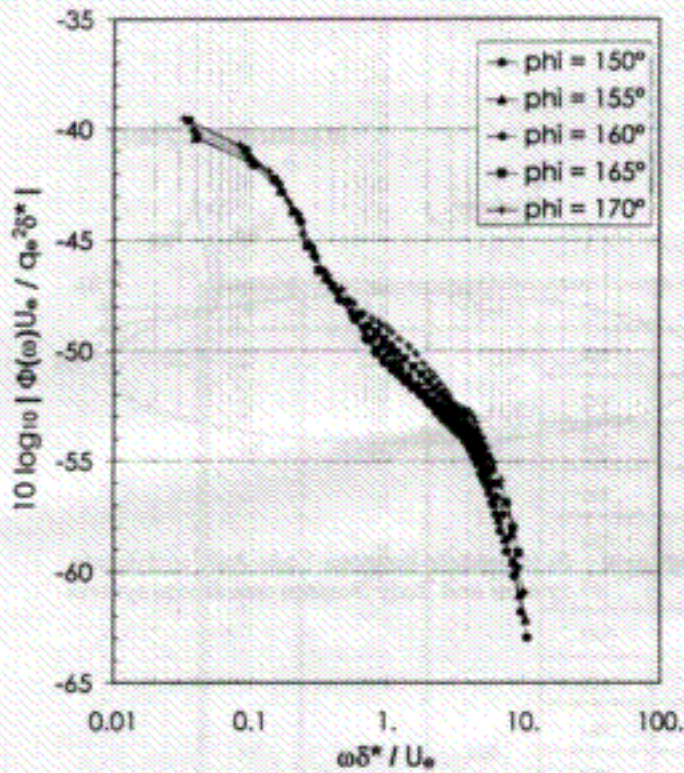


Figure 4 - Power spectra of wall pressure fluctuations scaled on  $\delta^*$ ,  $U_e$ , and  $q_w$ .  
 $\alpha = 10^\circ$   $x/L = 0.600$

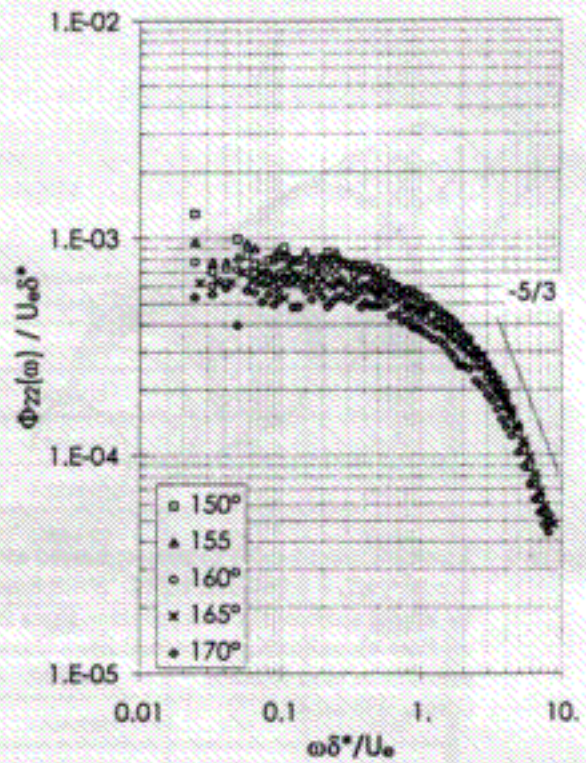


Figure 6 - Power spectra of velocity fluctuations (V component) scaled on  $\delta^*$ ,  $U_e$ .  
 $\alpha = 10^\circ$   $x/L = 0.600$   $r = 0.75$  cm

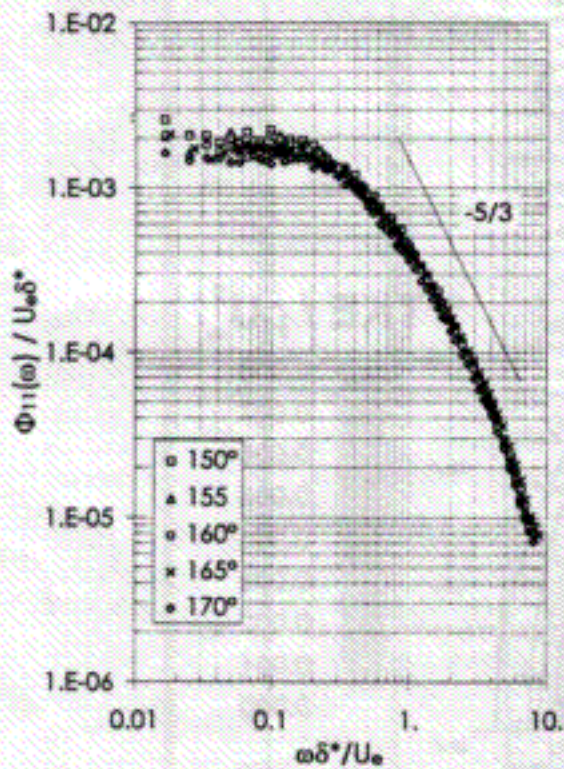


Figure 5 - Power spectra of velocity fluctuations (U component) scaled on  $\delta^*$ ,  $U_e$ .  
 $\alpha = 10^\circ$   $x/L = 0.600$   $r = 0.75$  cm

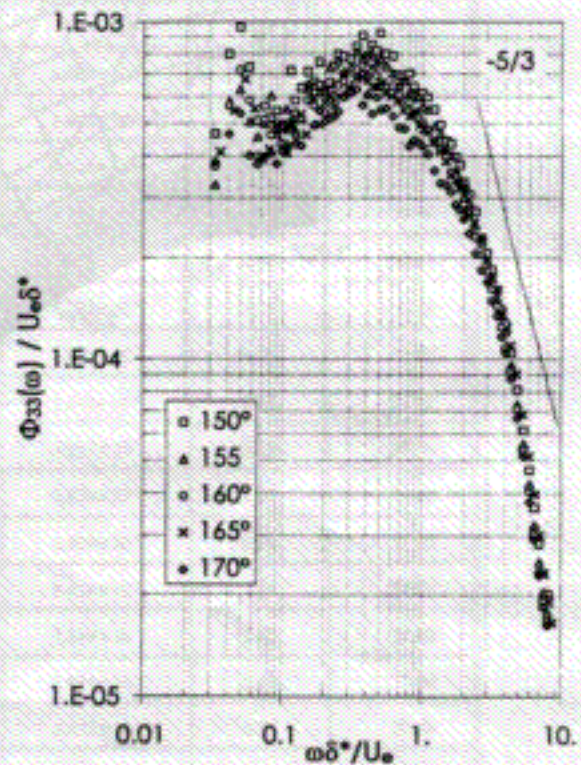


Figure 7 - Power spectra of velocity fluctuations (W component) scaled on  $\delta^*$ ,  $U_e$ .  
 $\alpha = 10^\circ$   $x/L = 0.600$   $r = 0.75$  cm

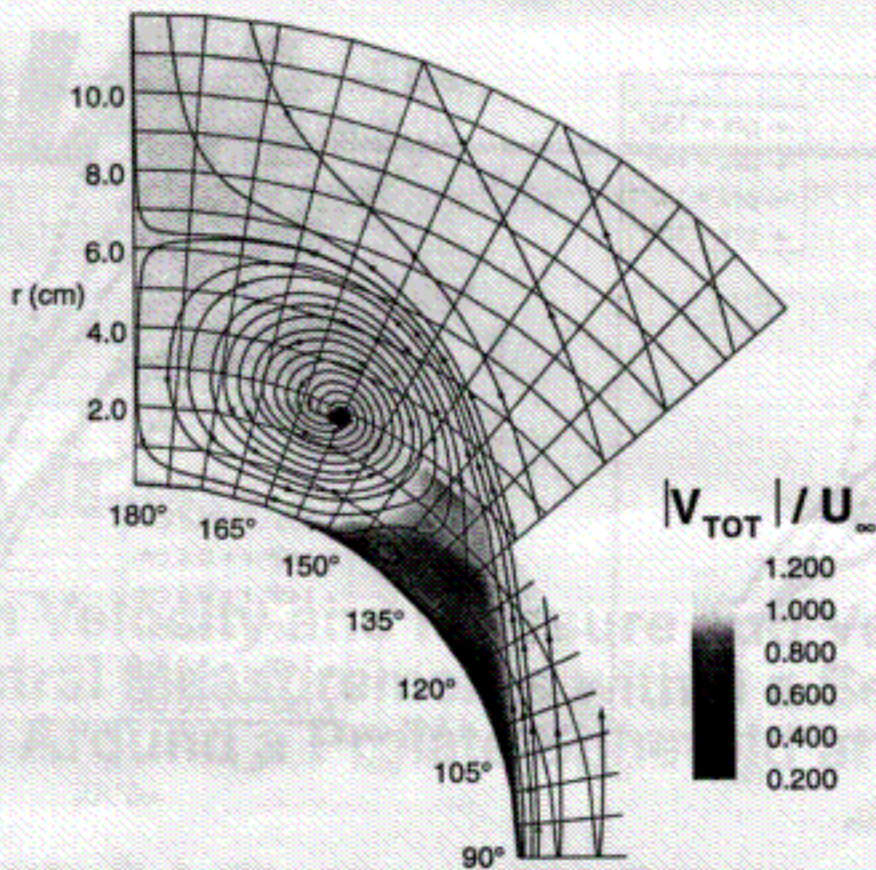


Figure 8 - Secondary streamlines with contours of (local mean velocity magnitude) /  $U_\infty$   
 $\alpha = 20^\circ$   $x/L = 0.772$

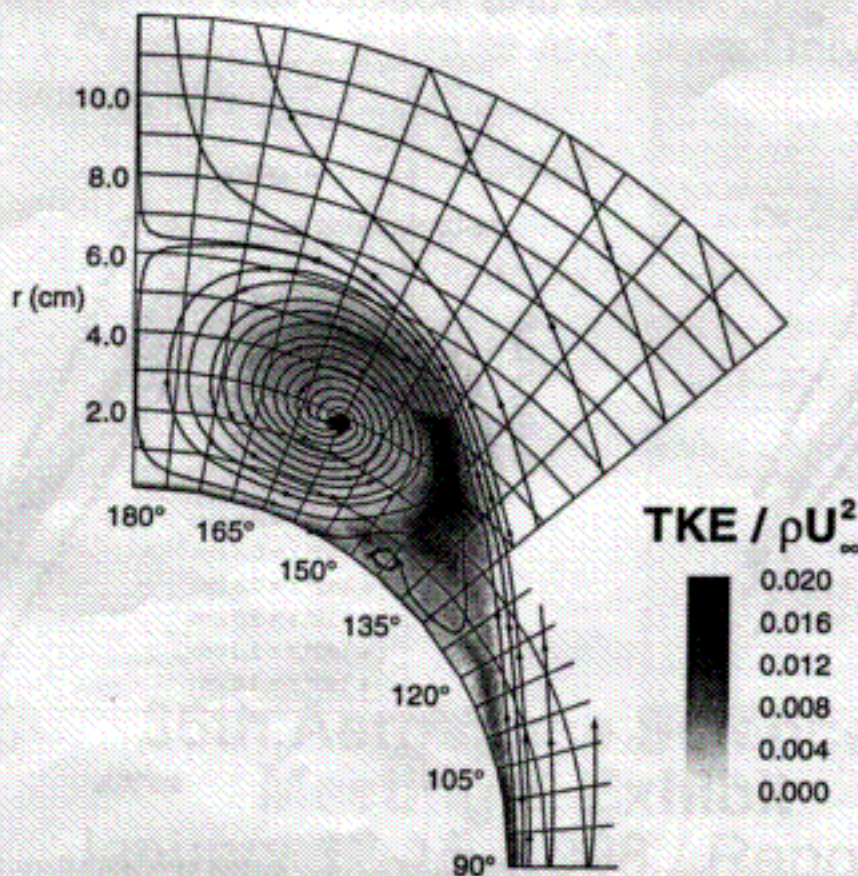


Figure 9 - Secondary streamlines with contours of (turbulent kinetic energy) /  $\rho U_\infty^2$   
 $\alpha = 20^\circ$   $x/L = 0.772$

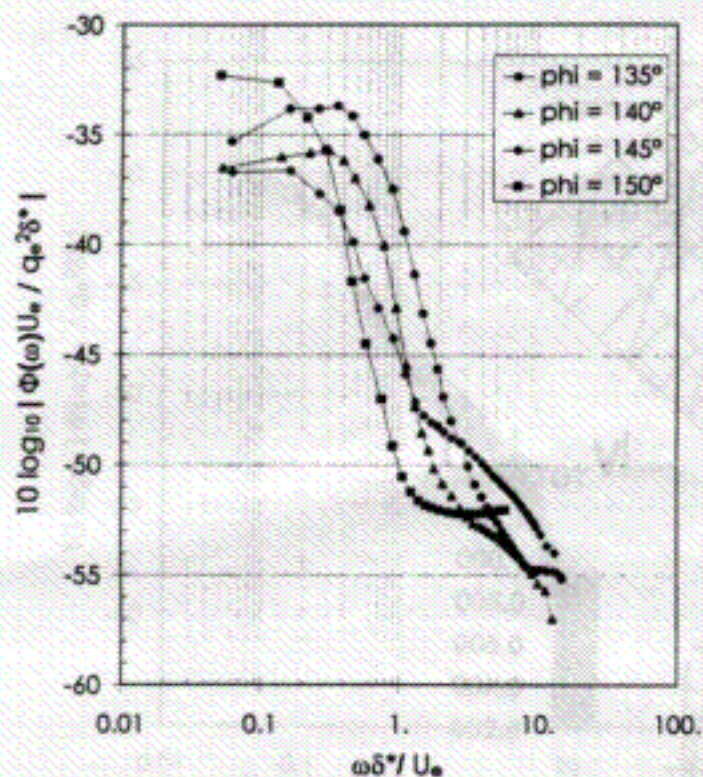


Figure 10 - Power spectra of wall pressure fluctuations scaled on  $\delta^*$ ,  $U_e$ , and  $q_e$ ,  $\alpha = 20^\circ$   $x/L = 0.772$

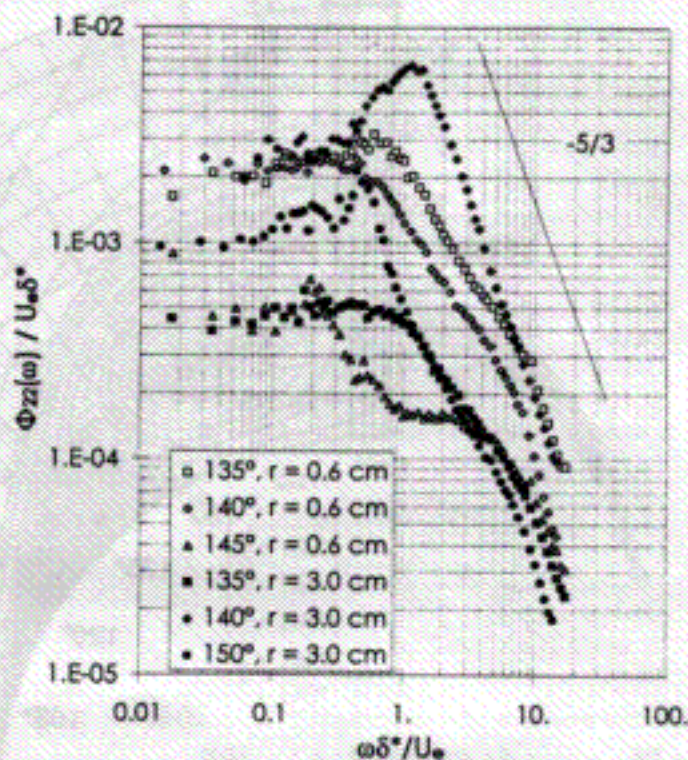


Figure 12 - Power spectra of velocity fluctuations (V component) scaled on  $\delta^*$ ,  $U_e$ ,  $\alpha = 20^\circ$   $x/L = 0.772$

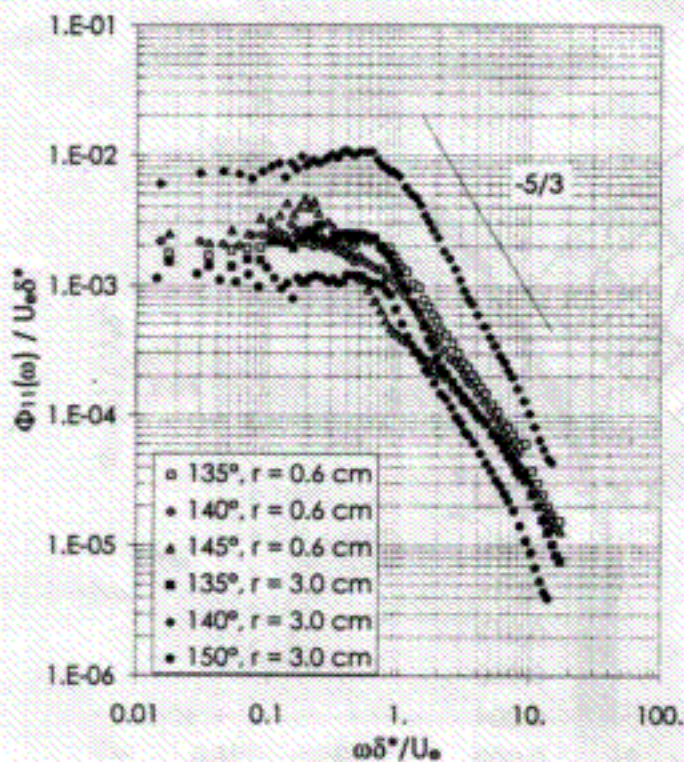


Figure 11 - Power spectra of velocity fluctuations (U component) scaled on  $\delta^*$ ,  $U_e$ ,  $\alpha = 20^\circ$   $x/L = 0.772$

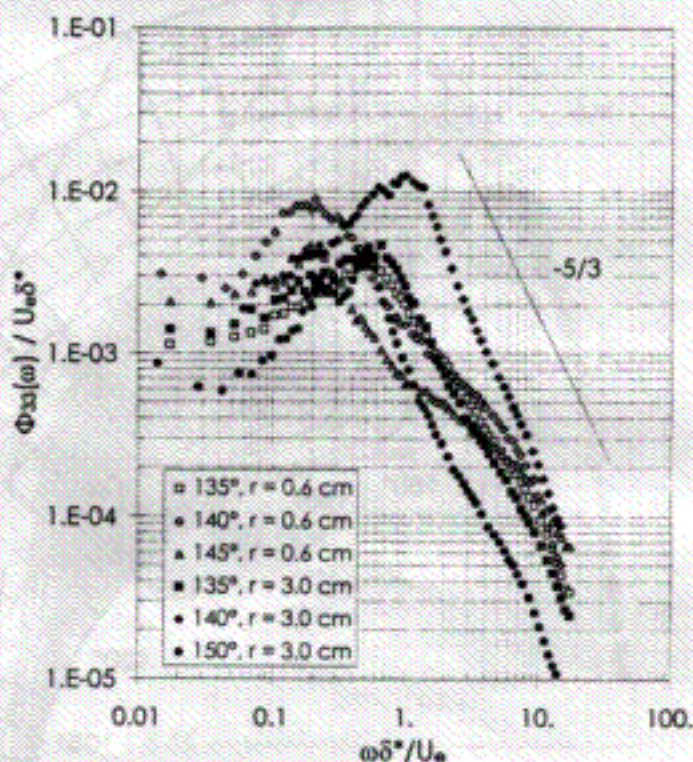


Figure 13 - Power spectra of velocity fluctuations (W component) scaled on  $\delta^*$ ,  $U_e$ ,  $\alpha = 20^\circ$   $x/L = 0.772$